The Li_xVPn_4 Ternary Phases (Pn = P, As): Rigid Networks for Lithium Intercalation/Deintercalation

Marie-Liesse Doublet,*,† Frédéric Lemoigno,† Frédéric Gillot,‡ and Laure Monconduit‡

CNRS−Laboratoire de Structure et Dynamique des Systèmes Moléculaires et Solides and CNRS−Laboratoire des Agrégats Métalliques et des Matériaux Inorganiques, Université Montpellier II, Bât. 15, Place Eugène Bataillon, 34 095 Montpellier Cédex 5, France

Received January 18, 2002. Revised Manuscript Received July 11, 2002

We present the ternary phases Li_xVPn_4 (Pn = P, As) as new materials for the negative electrode in lithium-ion batteries. Associated with a large variation of lithium content per formula unit ($3 \leq x \leq 7.5$ for P and $3 \leq x \leq 11$ for As), these materials show a higher specific capacities in their first charge/discharge cycle than the graphite (550 mA·h/g for Pn = P and 530 mA·h/g for Pn = As vs 372 m·Ah/g for C_{gr}) and open new routes for the design of new types of rechargeable Li-ion batteries. High-temperature syntheses, X-ray diffraction analyses, and first-principle electronic structure calculations give evidence of remarkable stability of the Li_xVPn_4 crystal structure upon various lithium compositions. Owing to rather strong covalent V−Pn bonds, the host matrixes behave as structurally stable networks of weakly interacting tetrahedra, able to store (respectively, release) a large number of additional electrons (correlatively with the intercalation (respectively, deintercalation) of Li^+ in the host matrix) into a nearly nonbonding Pn−Pn band. This leads to very weak volumetric variations (<1%) of the unit cells upon cycling compared to what is usually observed in the negative electrode materials such as alloy compounds. The cycling performances of the new, promising Li_xVPn_4/Li cells are currently under investigation.

1. Introduction

During the past 10 years, great interest has been devoted to rechargeable lithium batteries, particularly because they offer higher energy storage capacities than conventional batteries.[1] The current generation of lithium-ion batteries is designed with layered intercalation compounds such as transition metal oxides[2−4] for the positive electrodes and carbons[5,6] for the negative ones. From a fundamental aspect, a promising negative (respectively, positive) electrode material must combine both a high specific charge and a low (respectively, high) redox potential with respect to the reference Li/Li^+ redox reaction of the elemental lithium. For the Li-ion battery, these two requirements are met with a high number (x) of available charge carriers Li^+ per mass and volume units and a high cell voltage ($V_{cell} = V_{cathode} - V_{anode}$). Moreover, the electrochemical reactions occurring both at the positive and at the negative electrode have to be highly reversible to retain the specific charge capacity (C) upon hundreds of charge/discharge cycles.

To find promising electrode materials, the synthesis of new intercalation compounds exhibiting a rather low formula weight and a high lithium content variation (Δx) is the strategy to follow. Among the large number of new materials recently emerged in the litterature, alloying systems such as the Li_xM, where M = Al, Sn Si, Sb phases,[7−12] appear to be attractive materials. However, the severe volumetric variations occurring in these systems during the lithiation and the delithiation processes (up to 400% of the unit cell volume) keep limiting the electrode performances. To bypass the mechanical stresses induced by these volume changes and to increase the lifetime of the lithium-ion cell, it has been proposed to use composite electrodes such as Li_xSnO_y[13] in which an inactive component could buffer the volumetric variation of the active Li_xSn compound. Unfortunately, these systems suffer from an unacceptable irreversible capacity loss during the first cycle.[14,15]

* To whom correspondence should be addressed. E-mail: Marie-Liesse.Doublet@lsd.univ-montp2.fr.

† Laboratoire de Structure et Dynamique des Systèmes Moléculaires et Solides.

‡ Laboratoire des Agrégats Métalliques et des Matériaux Inorganiques.

(1) Kinoshita, K. In *New Trends in Electrochemical Technology*: *Energy Storage Systems for Electronic*; Osaka, T., Datta, M., Eds.; Gordon and Breach Sciences Publishers: Reading, U.K., 2000; p 193.

(2) Tarascon, J.-M.; Guyomard, D. *J. Electrochem. Soc.* **1991**, *138* (10), 2864.

(3) Ammundsen, B.; Jones, D.; Rozière, J.; Villain, F. *J. Phys. Chem. B* **1998**, *102*, 7939.

(4) Armstrong, A. R.; Bruce, P. G. *Nature* **1996**, *381*, 499.

(5) Flandois, S.; Simon, B. *Carbon* **1999**, *37*, 165.

(6) Yazami, R. *Electrochim. Acta* **1999**, *45*, 87.

(7) Yang, J.; Winter, M.; Besenhard, J. O. *Solid State Ionics* **1996**, *90*, 281.

(8) Besenhard, J. O.; Yang, J.; Winter, M. *J. Power Sources* **1997**, *68*, 87.

(9) Boukamp, B. A.; Lesh, G. C.; Huggins, R. A. *J. Electrochem. Soc.* **1981**, *128*, 725.

(10) Wang, J.; Raistrick, I. D.; Huggins, R. A. *J. Electrochem. Soc.* **1986**, *133*, 457.

(11) Besenhard, J. O.; Komenda, P.; Paxinos, A.; Wudy, E.; Josowicz, M. *Solid State Ionics* **1986**, *18−19*, 823.

(12) Besenhard, J. O.; Hess, M.; Komenda, P. *Solid State Ionics* **1990**, *40−41*, 525.

(13) Idota, Y.; Nishima, M.; Miyaki, Y.; Kubota, T.; Miyasaki, T. Eur. Pat. Appl. 651450A1950503, 1995.

10.1021/cm020047e CCC: $22.00
Published on Web 09/27/2002

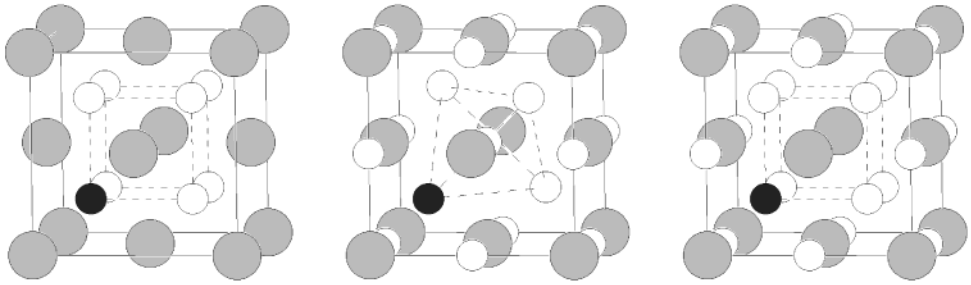

Figure 1. (a) Antifluorite-type (A) crystal structure; (b) filled zinc-blende (B) crystal structure; (c) filled antifluorite-type structure. The black, gray, and white circles correspond to the transition metal, the pnictogen, and the lithium atoms, respectively.

Thackeray and co-workers partially solved this problem with the Li_xInSb and $Li_xCu_6Sn_5$ intermetallic phases.[16,17] These materials exhibit much higher volumetric capacities than the lithiated graphite as well as small volumic changes and small irreversible capacities (compared to Li_xSnO_y). Hence, it seems that a strong structural relationship is required between the parent electrode and the lithiated compounds to avoid the dramatic structural damages caused by lithium intercalation/deintercalation.

In this work, we aim at showing that the transition metal pnictogenides Li_xVPn_4 (Pn = P, As) satisfy most of the structural and electronic requirements for ideal electrode materials. In particular, they exhibit higher specific capacities than the layered graphite in their first charge/discharge electrochemical cycle. These good electrochemical performances originate from the combination of a large variation of lithium content per formula unit, a strong structural stability of the host matrix in the whole range of lithium compositions, and an averaged intercalation/deintercalation potential close to 1 V. On the basis of high-temperature syntheses, X-ray diffraction (XRD) analyses, and first-principle electronic structure calculations, we show that the transition metal is mainly responsible for the high structural stability of these phases as well as for their remarkable electrochemical properties. One of the major drawbacks of these phases is the use of arsenic, which is obviously not environmentally friendly. Showing very close structural and electrochemical properties compared to the phosphides, the arsenides compounds are investigated here as model electrodes. In the next section, crystal structures and electrochemical properties of the ternary Li_xVPn_4 (Pn = P, As) are presented. Section 3 is devoted to electronic structure calculations and discussion. Conclusions and prospectives are summarized in section 4.

2. Crystal Structure and Electrochemical Properties of the Li_xVPn_4 (Pn = P, As)

The ternary phases Li_xVPn_4 (Pn = P, As) are known from the earlier work of Juza and co-workers[18] and were described within an antifluorite-type crystal structure (A) where the eight tetrahedral Pn-coordinated sites of the pnictogen fcc (face-centered cubic) unit cell are statistically filled with the lithium and the transition metal atoms in a 7:1 ratio (Figure 1a). In a purely ionic description of the chemical bond, a formal electron count leads to the general formula $Li_{2n-3}M^nPn_{n-1}$ in which the number of lithium atoms per unit cell is directly correlated to the formal oxidation state of the transition metal (n) and with the pnictogen anions in a Pn^{3-} formal state.[18c] A potential application as an electrode material is thus easy to forsee since additional lithium can be inserted into the Li_7MPn_4 systems to fill the available cationic vacancies of the pnictogen fcc bulk and to reduce the transition metal (Figure 1c).

2.1. Preparation of the Pristine Compounds. Recently, we reported high-temperature synthesis and XRD characterizations for several compounds of the same series,[19] that is, Li_7NbP_4, $LiNbAs_2$, and $Li_{4.5}V_{1.2}As_4$. In the present work, three novel phases are synthesized, namely, the Li_7VP_4, $Li_{2.3}V_{1.2}As_4$, and $Li_{9.3}VAs_4$. The synthesis is carried out inside a niobium tube sealed under argon by arc welding and for different concentrations of lithium. Powders of elements were used, except for lithium (metal chunks or Li_3Pn powder). Li_xVPn_4 alloys were prepared by melts of lithium or/and Li_3Pn and pnictogens in stoichiometric proportions that attack the refractory metal. They were heated at 900 °C for 20 h and cooled quite rapidly (100°/h) to prevent the formation of stable binary phases. Air- and moisture-sensitive starting materials and products were handled in an argon-filled glovebox. Initial characterizations of the reaction products were carried out using X-ray diffraction (XRD) patterns recorded on a Philips model diffractometer, using monochromated Cu Kα radiation. For the phosphide, they reveal the presence of Li_3P and VP_y impurities, in a rather large amount. Because no single crystal could be isolated, it was not possible to determine the accurate stoichiometry of the Li−V−P ternary phase obtained. From now on, it will thus be noted $Li_{\sim 7}VP_4$. For the arsenides, only single phases were obtained. Whenever it was possible, single crystals were isolated and analyzed to obtain structural information. This is the case for the poor lithiated $Li_{2.3}V_{1.2}As_4$ phase and for the previously reported $Li_{4.5}V_{1.2}$-

(14) Idota, Y.; Kubota, T.; Matsufuji, A.; Maekawa, A.; Miyasaki, T. *Science* **1997**, *276*, 1395.
(15) Courtney, I. A.; Dahn, J. R. *J. Electrochem. Soc.* **1997**, *144*, 2045.
(16) Vaughey, J. T.; O'Hara, J.; Thackeray, M. M. *Electrochem. Solid-State Lett.* **2000**, *3*, 13.
(17) Kepler, K. D.; Vaughey, J. T.; Thackeray, M. M. *Electrochem. Solid-State Lett.* **1999**, *2*, 307.
(18) (a) Juza, R.; Uphoff, W. *Z. Anorg. Allg. Chem.* **1957**, *292*, 65. (b) Langer, V.; Juza, R. *Z. Anorg. Allg. Chem.* **1968**, *361*, 74. (c) Juza, R.; Langer, K.; von Benda, K. *Angew. Chem. Int. Ed. Engl.* **1968**, *7*, 5.
(19) Monconduit, L.; Tillard-Charbonnel, M.; Belin, *C. J. Solid State Chem.* **2000**, *156*, 37.

Table 1. Unit Cell Parameters (esd in parentheses) as Well as Space Groups for the Synthezised Li_xVPn_4 (Pn=P, As) Phases. (* partial additional crystallographic data for single-crystal refinement)

	unit cell parameter *a* (Å)		
Li_xVPn_4	single crystal	powder	space group
$Li_{2.3}V_{1.2}As_4$	6.153(1)[a,b]	6.168(1)[a]	$F\bar{4}3m$
$Li_{4.5}V_{1.3}As_4$	6.167(1)[c]		$F\bar{4}3m$
Li_7VAs_4		6.159[d]	$Fm\bar{3}m$
$Li_{9.3}VAs_4$		6.175(2)[a]	$Fm\bar{3}m$
$Li_{9.6}V_{1.4}As_4$		6.151[e]	$Fm\bar{3}m$
Li_7VP_4		5.987[d]	$Fm\bar{3}m$
		5.970(1)[a]	$Fm\bar{3}m$
$Li_{9.8}V_{1.2}P_4$		5.977(1)[e]	$F\bar{4}3m$

[a] Present work. [b] Space group: $F\bar{4}3m$. Molecular weight ($g \cdot mol^{-1}$): 364.50. Lattice parameter (Å): 6.153(1). Cell volume ($Å^3$): 232.98. Calculated density ($mg \cdot m^{-3}$): 2.59. μ (mm^{-1}): 15.06. θ range (°): 5.74−49.24. Collected reflections (octant *hkl*): 358. Number of unique data with $I > 2\sigma(I)$: 89. Equivalent reflection averaging: $R_{int} = 8.49$. Number of refined parameters: 8. Goodness of fit: 1.05. R1 ($I > 2\sigma(I)$): 2.80; wR2 ($I > 2\sigma(I)$): 5.97. Residual electron densities: +0.81/−0.53. [c] Single-crystal refinement data can be found in ref 19. [d−e] Powder XRD analysis provided by Juza and co-workers in refs 18a and 18b, respectively.

As_4 one.[19] The results are presented in Table 1, along with those of previous works.

The most striking point is that neither the unit cell parameters ($\Delta a = 1\%$) nor the crystalline lattices (cubic type) change drastically with the lithium composition for both Li_xVPn_4 systems. Nevertheless, in addition to the antifluorite-type crystal structure, a partially filled zinc-blende type (B) crystal structure (Figure 1b) is used to describe the phases associated with low lithium compositions. On the basis of the same fcc bulk of pnictogen atoms, the latter (B) shows a different cationic distribution than the former (A), with half the tetrahedral and the octahedral Pn-coordinated sites partially filled with lithium and transition metal atoms. Note that whatever the cationic distribution in these structures, the transition metal always lies in a tetrahedral Pn-coordinated position, suggesting a greater stability for the MPn_4 tetrahedron than for the MPn_6 octahedron.

2.2. Electrochemical Measurements. Swagelok-type cells were assembled in an argon-filled glovebox and cycled using a Mac-Pile automatic cycling/data recording system (Biologic Co, Claix, France) between 2 and 0.01 V. They consist of a 0.4-cm^2 disk of composite electrode containing 7−10 mg of Li_xMPn_4 powder mixed of carbon black 4 N strem (10 wt %) and pressed into a pellet, a 0.3-cm^2 Li metal disk as a negative electrode, and a Whatman GF/D borosilicate glass fiber sheet saturated with a 1 M $LiPF_6$ electrolyte solution in 1:1 dimethyl carbonate:ethylene carbonate as the separator/electrolyte.

Our first galvanostatic closed circuit voltage (CCV) measurements are presented in Figure 2a, with the cell voltage (V_{cell}) of the Li_7VP_4/Li−metal and the $Li_{9.3}VAs_4$/Li−metal cells plotted as a function of the lithium content (*x*). They were started in oxidation (delithiation) from the $Li_{\sim 7}VP_4$ and $Li_{9.3}VAs_4$ initial compositions and the cells were cycled at scan rates C/34 (one lithium in 34 h) and C/9 (one lithium in 9 h) for Li−V−P and Li−V−As, respectively. These very low scan rates are used to ensure that the thermodynamical equilibrium can be assumed and that kinetic quantities such as lithium diffusivity is not a limiting factor for Li^+ intercalation/deintercalation. Note that a drastic increase of the lithium rates shows a significant drop of Δx for the two systems. The voltage curves reveal averaged cell voltages close to 1 V vs elemental lithium for both Li−V−P and Li−V−As sytems. This validates the potential use of these materials as negative electrodes. First, their intercalation/deintercalation potentials are higher than that of elemental lithium. This prevents the safety issues encountered in negative electrode materials exhibiting potentials vs lithium close to 0 V when the cells reach an overcharged state (due to lithium deposition). Second, the combination of these materials with the recently reported high potential transition metal oxides[20,21] or phosphates[22−24] still leads to rechargeable batteries with reasonable potential windows (3 or 4 V, respectively).

Thanks to the large lithium content variation ($\Delta x = 4.5$ for P and $\Delta x = 8.13$ for As), the two systems exhibit a high specific capacity of 550 mA·h/g for the Li_xVP_4 phase and 530 mA·h/g for the Li_xVAs_4 phase in the first charge/discharge cycle. This corresponds to volumetric capacities of 960 and 1560 $mA \cdot h/cm^3$, respectively. Note that the layered graphite shows a capacity limited to 372 mA·h/g (respectively, 820 $mA \cdot h/cm^3$). To our knowledge, reversible intercalation of such lithium amounts has never been reported for anodic materials. In contrast with what was expected by Juza et al.,[18c] poor lithium compositions are achieved by electrochemical routes for the two systems ($x = 3$). From the formal electron count they proposed, the vanadium oxidation state for the $Li_7V^{5+}Pn_4$ stoichiometry was not consistent with further oxidation, but with reduction only. This gives evidence of the formal electron count failure for such systems.

A flat potential is observed upon delithiation for the two cells, whereas the lithiation seems to proceed through either a classical single-phase process or a more complex one. From an academic point of view, the occurrence of a plateau in CCV curves is the signature of a two-phases process,[25] that is, a progressive decomposition of the pristine lithiated phase into a delithiated one. This is corroborated by potentiodynamic experiments performed on the $Li_{9.3}VAs_4$ electrode and presented in Figure 2b. The incremental capacity versus voltage curve clearly shows a sharp peak in oxidation, characteristic of the expected two-phases process. In reduction, three peaks of incremental capacity located at 1.0, 0.9, and 0.8 V are observed, suggesting a quite more complex mechanism during the discharge. The main question is then about the nature of the second phase, its crystal structure, and so the number of lithium truly inserted/deinserted in the host material.

At first guess, it would have been natural to believe that the ternary Li_xVPn_4 (Pn = P, As) phases partially decompose into the binary Li_3Pn ($Li_{12}Pn_4$) phases they

(20) Croguennec, L.; Pouillerie, C.; Mansour, A. N.; Delmas, C. *J. Mater Chem.* **2001**, *11*, 131.
(21) Tarascon, J.-M.; McKinnon, W. R.; Goowar, F.; Bowmer, T. N.; Amatucci, G.; Guyomard, D. *J. Electrochem. Soc.* **1994**, *141*, 1421.
(22) Anderson, A. S.; Kalska, B.; Häggström, L.; Thomas, J. O. *Solid State Ionics* **2000**, *130*, 41.
(23) Anderson, A. S.; Thomas, J. O. *J. Power Sources* **2001**, *97−98*, 498.
(24) Padhi, A. K.; Nanjundaswamy, K. S.; Goodenough, J. B. *J. Electrochem. Soc.* **1997**, *144*, 1188.
(25) Huggins, R. A. *Solid State Ionics* **1998**, *113*, 57.

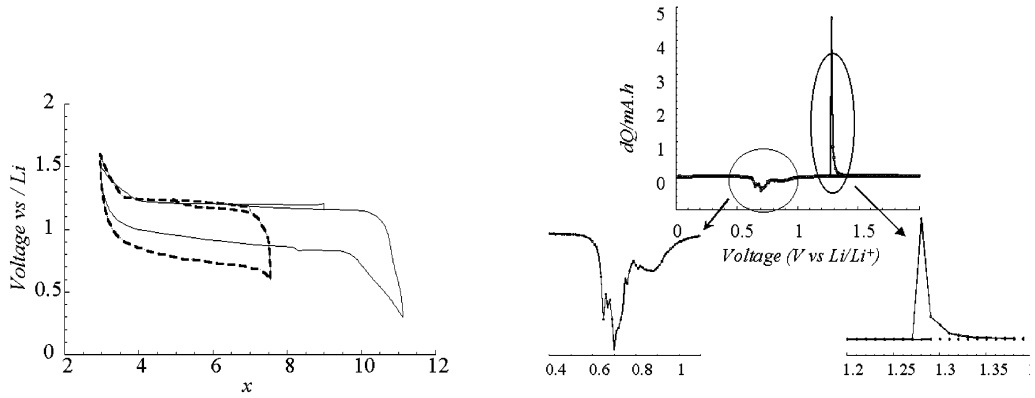

Figure 2. (a) Galvanostatic closed-circuit voltage (CCV) as a function of the lithium composition (x) for the Li_7VP_4/Li−metal (dotted) and the $Li_{9.3}VAs_4$/Li−metal (solid) cells. The cells were cycled starting in oxidation from the $Li_{9.3}VAs_4$ and $Li_{\sim 7}VP_4$ lithiated materials at the rates C/9 and C/34, respectively. (b) Potentiodynamic measurements for the $Li_{9.3}VAs_4$/Li−metal cell.

just structurally derive from. In the present case, this is very unlikely. First, it is difficult to figure out how, starting from $Li_{\sim 7}VP_4$ or from $Li_{9.3}VAs_4$, a second phase with a higher lithium concentration ($Li_{12}Pn_4$) could grow upon delithiation. Second, an ex situ XRD analysis carried out at the end of charge (using an air-proof sampler) did not detect any structural phase transition in the electrode. Though, the binary Li_3Pn (Pn = P, As) phases crystallize in hexagonal lattices.[26] Another hypothesis would be that the second phase growing in the electrode is amorphous. To address this question, an accurate in situ XRD analysis is required. Thus, it seems that the two-phases process could here correspond to the coexistence of two phases with very different lithium compositions but equivalent Laue lattices, that is, equivalent host matrixes.

This hypothesis is consistent with our previous XRD analyses that pointed out the stability of poor $Li_{2.3}V_{1.2}As_4$ and rich $Li_{9.3}VAs_4$ lithiated phases in nearly equivalent fcc cells. Because small stoichiometry deviations are observed for the transition metal, it is difficult to accurately quantify the lithium composition dependence of the unit cell parameter. Nevertheless, it should not be significant. Which of the fcc lattice or the VPn_4 network is responsible for this stability and does the cationic distribution (A vs B) influence the lithium intercalation/deintercalation mechanisms in these ternary phases are the two fundamental questions we will now focus on.

3. Electronic Structure Calculations

3.1. Computational Details and Models. First-principle calculations based on the density functional theory (DFT) formalism were performed on the Li_xVPn_4 (Pn = P, As) systems. The Amsterdam Density Functional package for periodic systems (ADF-Band)[27] was used for different lithium stoichiometries varying from $x = 0$ to $x = 11$. To ensure a better treatment of the electronic repulsions, the gradient-corrected functional of Perdew−Wang[28] was used for the exchange-correlation energy. For each lithium composition, the different cationic distributions in both the tetrahedral and the octahedral Pn-coordinated sites were investigated in fixed VP_4 and VAs_4 bulk, using the unit cell parameters refined from our single-crystal and powder XRD analyses. Although more rigorous calculations would imply geometry relaxations for each lithium composition and each cationic distribution, such a structural approximation is legitimated by our XRD results and by the fact that no energy-sensitive physical magnitudes (such as electrochemical potential calculations for instance) will be investigated in this work. Rather, density of states (DOS) as well as crystal orbital overlap populations (COOP) for the V−Pn and Pn-Pn bonds will be used to show that the different lithium compositions and distributions induce different electron density rearrangements that are likely responsible for the high structural stability of the VPn_4 (Pn = P, As) networks. Provided by a Mulliken[29] analysis, the COOP curves display the bonding (COOP > 0), nonbonding (COOP ∼ 0), and antibonding (COOP < 0) character of one given local bond in the whole range of energy. The summation of these COOP curves over all the occupied states leads to integrated values (namely, the ICOOPs) that have already proved to be rather good bond strength indicators.[30,31] Nevertheless, since the Mulliken-type analyses are known to suffer from basis-set dependencies as well, it was necessary to supply our results with electron density plots. These were computed using the full-potential linearized augmented plane waves (FLAPW) code WIEN97.[32] This DFT program package, despite its somehow arbitrary partition of space between atomic spheres and interstitial regions, does not introduce approximation in the shape of the potential and in the charge density, thanks to linearization. The generalized gradient approximation (GGA)[33] was used for all cal-

(26) von Benda, K.; Juza, R. *Z. Anorg. Allg. Chem.* **1969**, *371*, 172.
(27) Te Velde, G. Ph.D. Thesis, Vrije Universiteit, Amsterdam, 1990. Te Velde, G.; Baerends, E.-J. *Phys. Rev. B* **1991**, *44*, 44. Te Velde, G.; Baerends, E.-J. *Phys. Rev. B* **1991**, *44*, 7888.
(28) Perdew, J. P.; Wang, Y. *Phys. Rev. B* **1992**, *45*, 244.
(29) Mulliken, R. S. *J. Chem. Phys.* **1955**, *23*, 1833.
(30) Dronskowski, R.; Blöchl, P. E. *J. Phys. Chem.* **1993**, *97*, 8617.
(31) Doublet, M.-L.; Remy, S.; Lemoigno, F. *J. Chem. Phys.* **2000**, *113*, 13.
(32) Blaha, P.; Schwarz K.; Luitz, J. *WIEN97, A full potential linearized augmented plane wave package for calculating crystal properties*; Karlheinz Schwarz, Techn. Universität Wien: Austria, 1999; ISBN 3-9501031-0-4 (An improved version: Blaha, P.; Schwarz, K.; Sorantin, P.; Trickey, S. B. *Comput. Phys. Commun.* **1990**, *59*, 399).
(33) Perdew, J. P.; Burke, S.; Ernzerhof, M. *Phys. Rev. Lett.* **1996**, *77*, 3865.

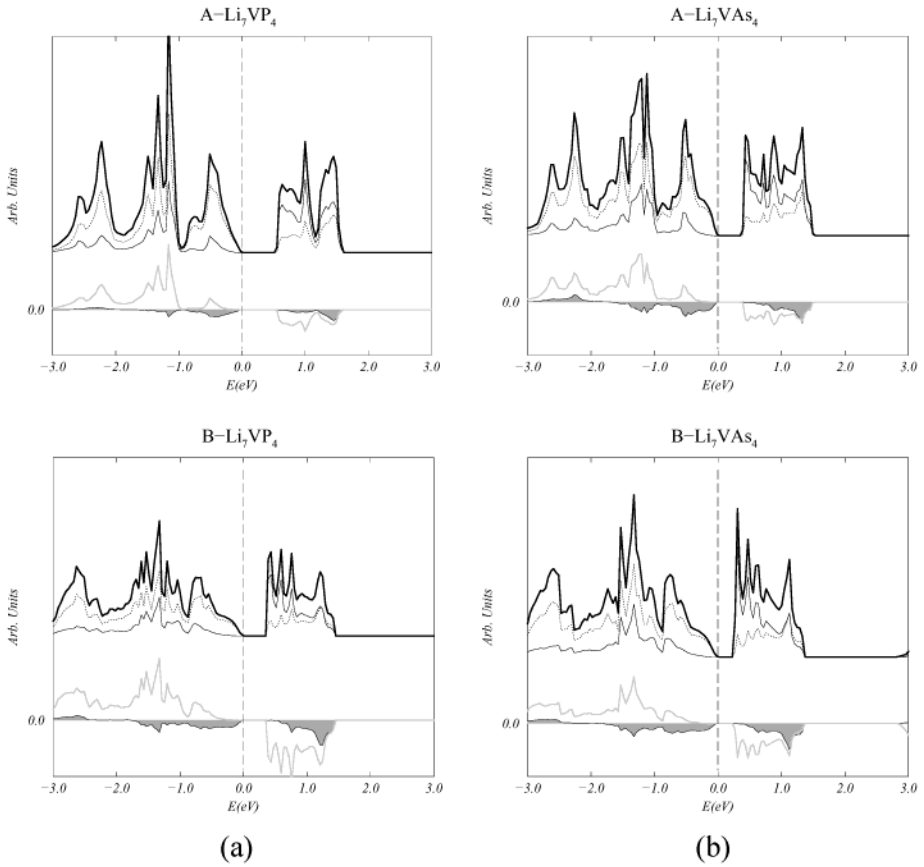

Figure 3. Density of states (upper part) as well as V−Pn and Pn−Pn (Pn = P, As) crystal orbital overlap populations as a function of the energy, for the ideal Li_7VP_4 (a) and Li_7VAs_4 (b) systems for both the A-type and B-type cationic distributions. The solid, dotted, and thin lines correspond to the total DOS and the partial DOS projected on the transition metal and the partial DOS projected on the pnictogen, respectively. The gray COOP corresponds to the V−Pn bonds and the filled one to the Pn−Pn bonds. The dashed vertical line stands for the Fermi level.

culations with a 1585 plane waves basis set, up to 600 eV to reach the convergence of calculations.

3.2. Influence of the Transition Metal. Our first goal is to check whether the transition metal plays a pure ionic role in the electronic structure of the fcc lattice, as suggested by the formal electron count proposed by Juza et al.,[18c] or if it imposes a strong deformation of the electron density to form covalent V−Pn bonds and therefore VPn_4 tetrahedra, as suggested by the stability of the phases toward various lithium compositions. The DOS and COOP presented in Figure 3 clearly show that the electronic structures of the Li_7VPn_4 (Pn = P, As) phases resemble more those of weakly interacting tetrahedra than those of *fcc* bulk, doped with localized M^{5+} and Li^+ cations. The low-lying filled band directly comes from the bonding V−Pn molecular levels, while the high-lying empty one is built on the antibonding V−Pn ones. Consequently, the Pn−Pn COOPs are much smaller in magnitude than the V−Pn ones in the whole range of energy, suggesting that the electron density is mainly localized along the V−Pn bonds rather than between the tetrahedra. Both ICOOPs and electron density plots (Table 2 and Figure 4, respectively) confirm this picture. The very different V−Pn and Pn−Pn bond strengths obtained by integrating the COOP curves up to the Fermi level are corroborated by the contour plots of Figure 4. They clearly illustrate that the vanadium valence density is distorted toward the four surrounding phosphor atoms. This is the signature of a covalent V−P bond character. Note that equivalent results are obtained for the Li_7VAs_4 system.

Table 2. Atomic Mulliken Populations and Integrated-COOP Values for the V−Pn and the Pn−Pn Bonds, Calculated for Different Lithium Concentrations of the Li_xVPn_4 (Pn = P, As) Phases as Well as Different Cationic Distributions over the Tetrahedral and Octahedral Pn-Coordinated Sites of the fcc Lattice[a]

	Mulliken population		ICOOP	
$Li_n^{Oh}Li_m^{Td}VPn_4$	V	Pn	V−Pn	P−Pn
$Li_0Li_3VP_4$	4.93	5.31	0.72	0.01
$Li_0Li_7VP_4$ (A)	5.32	5.48	0.68	−0.03
$Li_4Li_3VP_4$ (B)	5.09	5.45	0.64	−0.08
$Li_{12}P_4$ cubic		5.54		−0.15
$Li_0Li_3VAs_4$	4.85	5.35	0.70	0.01
$Li_0Li_7VAs_4$ (A)	5.01	5.76	0.66	−0.05
$Li_4Li_3VAs_4$ (B)	4.86	5.61	0.54	−0.10
$Li_{12}As_4$ cubic		6.19		−0.24

[a] The calculations have been performed within the generalized gradient approximation of Perdew−Wang.

The main role of the transition metal in these phases is thus to polarize the electron density inside the VPn_4 coordination sphere and therefore to partially isolate tetrahedra from each other. As a matter of fact, a much smaller distortion exists between the phosphor atoms located at the summits of each VP_4 tetrahedron, indicating weaker interactions between the neighboring VP_4 units. In contrast, in hypothetical $Li_{12}Pn_4$ binary cubic phases (isostructural to the ternary Li_7VPn_4 and as-

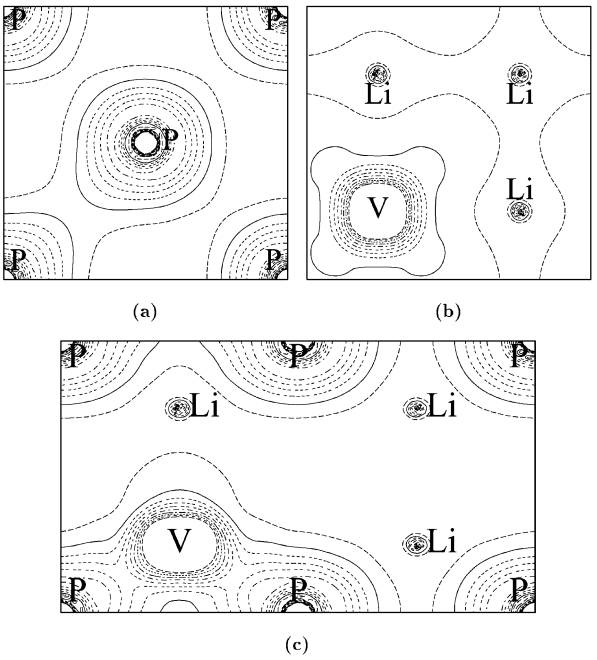

Figure 4. A-Li_7VP_4 density maps: (a) fcc cell face; (b) plane parallel to the cell face and passing through V; (c) plane directed by the z and $(x + y)$ axes.

sociated with an equivalent formal electron count for the fcc cell), a strong destabilization of the Pn−Pn bonds is observed. This supports the fact that binary phases do not crystallize in cubic lattices[26] and shows that the polarization induced by the transition metal on the electron density is essential for the stabilization of a cubic-type crystal structure.

3.3. Influence of the Lithium Composition and Distribution. In a rigid band hypothesis**,** where the band shape is kept constant whatever the electron filling, it is straightforward that the V−Pn and Pn−Pn bonds should be affected by the release or the addition of electrons, respectively, from and into the Li_7VPn_4 electronic structures. As reflected by the DOS and COOP (Figure 3), removing few electrons from the top portion of the highest filled band should strengthen the Pn−Pn bonds, keeping the V−Pn ones almost unchanged, while adding few electrons in the bottom portion of the first empty band should weaken the V−Pn bonds, keeping the Pn−Pn ones almost unchanged. These structural distortions are not consistent with our XRD results. To check the influence of both the cationic filling and the cationic distribution, it is thus necessary to go beyond the rigid band model and to compare the DOS and COOP curves as well as the electron density contour plots calculated for different lithium compositions and distribution.

From Li_3VP_4 to Li_7VP_4. As shown Figures 4 and 5, the electron density around vanadium and phosphor stretches out further as x raises from 3 to 7 (the same is observed for the Li−V−As system). This is in agreement with the reduction of V and Pn upon lithium intercalation and with the atomic Mulliken charges reported in Table 2. However, although a strengthening of the V−Pn bonds could be expected (by the rigid band model) from the DOS plots given in Figure 3, the V−Pn ICOOPs slightly decrease from $x = 3$ to $x = 7$. This is confirmed by the charge density map difference reported

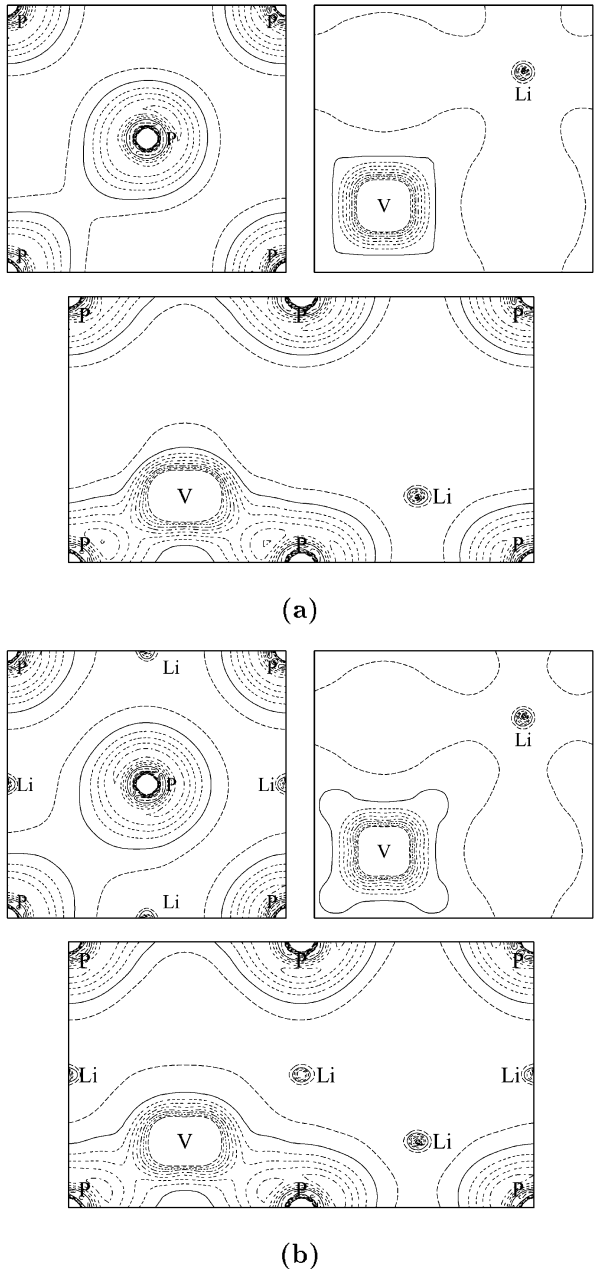

Figure 5. (a) Li_3VP_4 and (b) B-Li_7VP_4 density maps. The planes are the same as those in Figure 4.

in Figure 6a. Obtained by subtracting the electron density of A-Li_7VP_4 from that of Li_3VP_4, this plot shows a slight charge density depletion along the V−P bonds when lithium is inserted in the host material. These results stand true for the Li_xVAs_4 phases and show that the extra-charge density provided by the additional electrons from $x = 3$ to $x = 7$ does not localize on the V−Pn bonds but is instantaneously polarized inside the cubic cell, thanks to the intercalation of highly polarizing Li^+ cations. From a molecular point of view, such a deformation of the electron density is achieved through a metal to ligand back-donation. To minimize the electronic repulsions caused by the extra electrons between the transition metal and its surrounding ligands, an electron transfer occurs from the transition metal d-orbitals to the ligand empty lone pairs. The increase of the pnictogen charge density is further compensated by a polarization toward the Li^+ cations.

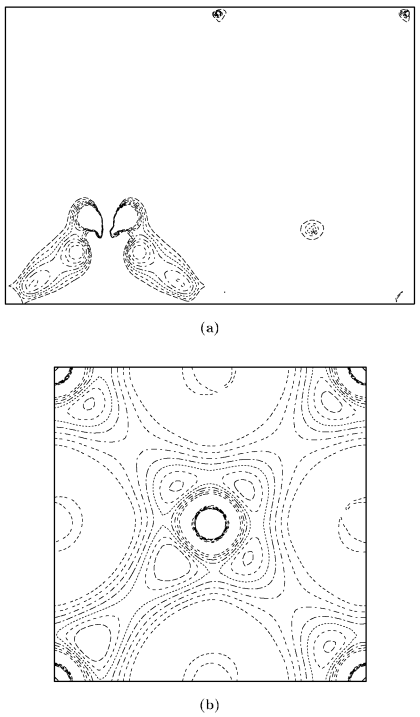

Figure 6. Density map differences (positive contours): (a) Li_3VP_4 minus A-Li_7VP_4 and (b) B-Li_7VP_4 minus A-Li_7VP_4.

This mechanism can obviously be achieved as long as available space inside the fcc lattice exists. Showing that the VPn_4 tetrahedra are not that much affected by the electron filling and therefore by the lithium composition of the Li_xVPn_4 bulk from $x = 3$ to $x = 7$, this analysis explains the very small variation of the VPn_4 cells upon lithiation/delithiation.

A-Li_7VPn_4 vs B-Li_7VPn_4. Considering the electronic structures calculated for A-Li_7VPn_4 and B-Li_7VPn_4 (Figure 3a for P and Figure 3b for As, respectively), significant differences are observed in the highest filled band shape. This clearly evidences the rigid band model limitation and suggests that the Li^+ cations do not polarize the electron density of the VPn_4 tetrahedra in the same manner depending on the site they occupy. As depicted in Figures 4 and 5, there is no noticeable charge density between lithium and phosphor whatever the type (tetrahedral or octahedral) of cationic site considered. Moreover, the electron density around lithium keeps an atomic-like, that is, spherical shape, characteristic of a highly ionic character of lithium in all cases. Nevertheless, the charge density map difference reported in Figure 6b reveals interesting features: the subtraction of the A-Li_7VP_4 charge density from the B-Li_7VP_4 one clearly shows that the electrons provided to the VP_4 hosts in a B-type cationic distribution mostly increase the P charge distribution on the fcc faces. This is corroborated by the Pn−Pn ICOOPs that exhibit a greater antibonding character in the B-type structure than in the A-type one and suggests that different electron transfers occur in the VPn_4 networks depending on the cationic distribution. It also suggests that the fcc cell might be more affected by lithium insertion/deinsertion than the VPn_4 tetrahedra.

To find out the origin of these electron transfers, it is necessary to pay a great deal of attention to the electrostatic interactions occurring in the Li_xVPn_4 bulk.

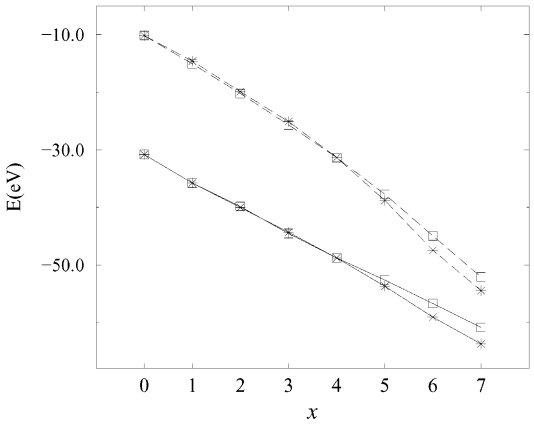

Figure 7. Electrostatic (dotted lines) vs total cohesive energies (solid lines) for the Li_xVP_4 systems ($0 = x = 7$) calculated within a fixed VP_4 host for progessive lithium filling within an A-type (stars) and B-type (squares) arrangement. For sake of clarity, the cohesive energies have been lowered by 10 eV.

In the A-type crystal structure, the next-nearest cation−anion (Li−Pn, V−Pn) and cation−cation (Li−V, Li−Li) distances are respectively shorter and longer than those in the B-type one (see Figure 1). From a basic electrostatic point of view, the A-type crystal structure should be preferred to the B-type one as the number of short cation−cation contacts increase. A more interesting result is that the total cohesive energies vary like the electrostatic ones for the two systems (Figure 7). It means that the relative thermodynamical stability of the two cationic distributions (A and B) is primarily governed by the electrostatics as far as lithium compositions close to 7 are concerned. For low lithium compositions, both the tetrahedral and the octahedral Pn-coordinated sites should be randomly reached by the Li^+ cations, to stabilize the charge of the VPn_4 anions. For higher lithium compositions, a progressive diffusion from the octahedral to the tetrahedral Pn-coordinated sites should occur to minimize the cation−cation repulsive interactions, hence yielding the A-type distribution and therefore a polarization of the electron density inside the cube. These results are crucial regarding the lithium intercalation/deintercalation mechanisms, showing that different site-ordered phases could be electrochemically achieved depending on whether the kinetics or the thermodynamics govern. If the tetrahedral Pn-coordinated sites are clearly favored by the thermodynamics, it is not that clear which of the tetrahedral or octahedral sites will be favored by the kinetics. Indeed, Li^+ cations are not required to go through a face of the fcc lattice to occupy the octahedral sites.

These results raise the question of a possible intercalation of more than seven Li^+ cations in the host material, as previously suggested by Juza and coworkers[18] and observed in the CCV curve of $Li_{9.3}VAs_4$/Li−metal (Figure 2). Indeed, from $x = 7$ to $x = 11$, the number of short cation−cation contacts increases rapidly and should become strongly destabilizing for the systems.

From Li_7VPn_4 to $Li_{11}VPn_4$. As shown on the DOS plots in Figure 3, the band involved in the electron transfers for $x > 7$ is very different from that involved in the electron transfers from $x = 3$ to $x = 7$. It consists of antibonding V−Pn electronic levels with a greater metallic contribution. Hence, additional electrons pro-

vided to the host material from $x = 7$ to $x = 11$ do not localize any longer along the V−Pn bonds but mostly around the transition metal. This means that some of the cation−cation repulsive interactions should be partially screened, thus allowing lithium compositions higher than 7. Needless to say, this screening effect will be as efficient as the unit cell is large. This is consistent with our electrochemical results since the $Li_{9.3}VAs_4$ system ($a = 6.175(2)$ Å) reaches higher lithium compositions than the Li_7VP_4 one ($a = 5.970(1)$ Å).

3.4. Discussion. We showed that the transition metal is responsible for both the stabilization of a cubic lattice and the very small variations of the Li_xVPn_4 unit cell parameters in the whole range of lithium compositions. An equivalent volumetric expansion upon charge/discharge has already been reported for the same cubic-type Li_xInSb intermetallic electrode material.[16] The plateau observed upon delithiation from $Li_{\sim 7}VP_4$ and $Li_{9.3}VAs_4$ is thus claimed to be the signature of a phase transformation, involving two phases that share the same VPn_4 network and differ only from their lithium composition and distribution. It is consistent with the fact that, although a thermodynamical equilibrium can be assumed, oxidation (delithiation) and reduction (lithiation) processes in Li_xVPn_4/Li−metal cells occur at different potentials. Indeed, we have shown that the thermodynamical stability of one given cationic composition depends on the cationic distribution. So if one follows the formulation of Ceder and co-workers[34] to calculate averaged electrochemical potentials (cohesive energy difference between two given compositions), it is possible to reach different potentials as far as different cationic distributions are considered. This tends to support the theory that different site-ordered phases are achieved upon discharge/charge, and therefore different intercalation/deintercalation mechanisms. One possible explanation could be related to the mode of synthesis used for the pristine compounds. It is likely that the experimental conditions imposed for the synthesis of the lithiated compounds (heating followed by a rapid cooling) are responsible for a different cationic distribution than that obtained upon electrochemical lithiation. At this stage, further cycling experiments are required to address this question. In particular, it should be interesting to study the cycling life of these Li_xVPn_4/Li−metal cells to check whether second and additional charge/discharge cycles keep the same shape. It would also be relevant to carry out galvano- and potentiodynamic intermittent titration techniques (GITT, PITT) to force a complete relaxation of the systems upon cycling, thus setting free the kinetics.

(34) Aydinol, M. K.; Kohan, A. F.; Ceder, G.; Cho, K.; Joannopoulos, J. *Phys. Rev. B* **1997**, *3*, 1354.

Conclusion

We have investigated the electrochemical performances of the Li_xVPn_4 ($3 \leq x \leq 11$, Pn = P, As) systems to be used as negative electrode materials in the rechargeable lithium-ion batteries. The first discharge/charge specific (respectively, volumetric) capacities of the Li_7VP_4/Li−metal and $Li_{9.3}VAs_4$/Li−metal cells are 550 and 530 mA·h/g (respectively, 960 and 1560 mA·h/cm^3), respectively. This is remarkable regarding the 372 mA·h/g (820 mA·h/cm^3) capacity reported for the layered graphite. The various Li_xVPn_4 phases synthesized at high temperature have given evidence of real structural stability of the VPn_4 networks toward various lithium compositions, a point that is crucial for the cell cycling life. First-principle electronic structure calculations have shown that the covalent VPn_4 tetrahedra as well as the large available volume provided by the cubic lattices are responsible for this stability. Moreover, electrostatic energies, density of states, and electron density analyses have revealed that different cationic distributions over the tetrahedral and octahedral Pn-coordinated sites induce different polarizations of the VPn_4 electron density. Different site-ordered phases, sharing the same crystallographic VPn_4 networks but exhibiting different thermodynamical stabilities, can thus be stabilized depending on both the lithium composition and the mode of synthesis (high temperature or electrochemical). This suggests that different lithium intercalation/deintercalation mechanisms should occur in the electrode depending on the initial cationic distribution of the pristine compounds and whether the kinetics or the thermodynamics govern. Of course, arsenide compounds cannot be seriously considered for such application. They were studied here as model electrodes. Since phosphides and arsenides are expected to be electronically and structurally close, efforts now deserve to be focused on the synthesis of other transition metal phosphides, Li_xMP_4, compounds to achieve more homogeneous reaction products and, hopefully, even better electrochemical performances.

Acknowledgment. M.-L.D. and L.M. would like to thank J.-M. Tarascon (Amiens, France), D. Guyomard (Nantes, France), and F. Favier (Montpellier, France) for useful discussions and support.

CM020047E